Journal of The Electrochemical Society, **147** (5) 1787-1796 (2000)
S0013-4651(99)05-090-9 CCC: $7.00 © The Electrochemical Society, Inc.

Formation Mechanisms and Characterization of Black and White Cobalt Electrodeposition onto Stainless Steel

Enrique Barrera,[a] Manuel Palomar Pardavé,[b,*] Nikola Batina,[c] and Ignacio González[c,,z]**

[a]*Departamento de Ingeniería de Procesos e Hidráulica, Área de Ingeniería en Recursos Energéticos and* [c]*Departamento de Química área de Electroquímica, Universidad Autónoma Metropolitana-Iztapalapa, C.P. 09340, México, D.F., Mexico*
[b]*Departamento de Materiales, Área de Ciencia de los Materiales, Universidad Autónoma Metropolitana-Azcapotzalco, C.P. 02200, México D.F., Mexico*

Cobalt electrodeposition onto a stainless steel substrate from 1.17 M Co(II) aqueous solution containing 0.98 M H_2SO_4, 0.56 M KCl, and 0.2 M H_3BO_3 was evaluated in the absence (*i*) and presence (*ii*) of 0.1 M KNO_3. Cobalt electrodeposited from the electrolytic bath (*i*) was white-gray colored, whereas deposition from bath (*ii*) formed a black-colored surface. SEM-WDX, AFM, and XRD analysis of the steel surfaces covered with these two deposits revealed distinct characteristics for black and white cobalt films. Although both deposits were composed of metallic cobalt, the white cobalt deposit was a smooth, 2D film while the black deposit consisted of many dispersed, nano-sized clusters of 150 to 250 nm in diameter. Analysis of potentiostatic current transients (*I-t* curves) indicated that formation of white cobalt was carried out by multiple 3D nucleation limited by lattice incorporation of cobalt adatoms to the growth centers. Formation of black cobalt was shown to involve the simultaneous processes of 3D nucleus formation and growth, limited by mass transfer, and the reduction of nitrates in the medium onto the surfaces of these nuclei. It is shown that, beside this cobalt-nitrate interaction, NO_3^- ions in solution can block active sites for cobalt reduction and the effect of this phenomenon strongly depends on the nitrate concentration. These facts could explain the observed dispersion of the black cobalt coating.

Manuscript submitted May 24, 1999; revised manuscript received December 15, 1999.

Photothermal conversion of solar energy to generate electricity is currently one of the most extensively applied techniques for harvesting solar energy worldwide. A major goal of companies devoted to the generation of power from solar energy photothermal conversion is the development of more competitive processes to reduce energy costs through improvement of the thermal performance of solar collectors.[1] Such improvements demand the use of solar collectors formed using highly efficient surfaces with high solar absortance (α) and low thermal emittance (ϵ). The former characteristic is required in order to collect the maximum possible incident solar energy in the collector lot and the latter to reduce energy losses due to heat radiation. Coatings formed from black metals (*i.e.*, black cobalt, black chromium, black nickel) have been shown to form fairly efficient collector surfaces, fulfilling the prescribed characteristics.[1,2] Several techniques, such as chemical conversion and/or thermal oxidation of metallic films and electrodeposition, are currently used to achieve such spectrally selective, black-metal, solar absorber surfaces. However, the desired characteristics of the metallic coating could be better controlled by directed electrodeposition.

Therefore, we propose to use electrodeposition to prepare a cobalt photothermal material suitable for use in solar energy collection. The mechanisms of electrochemical deposition for such a coating must be defined to enable preparation of materials with the required optical properties. In order to achieve control and reproducibility for the coating to qualify as an industrially useful material, the deposition process, as well, must be properly characterized.

We previously produced a black cobalt deposit with adequate optical properties for the photothermal conversion of solar energy.[2] This deposit was obtained by modifying the composition of an electrolytic bath for white cobalt production through the addition of a small amount of potassium nitrate (0.1 M). We reported the composition of the electrolytic bath required to produce black cobalt using a Hull cell. One of the main goals of our present work is to describe the mechanism of black and white cobalt deposition onto stainless steel and the role of nitrate in black cobalt formation.

Cobalt deposition has been carried out on substrates such as nickel, vitreous carbon, and copper, and from different electrolytic baths containing chloride or sulfate aqueous solutions,[3,4] triethylenediamine cobalt(III) chloride in 30% KOH, solutions of cobalt(II) thiocyanate in *N*,*N*-dimethyl formamide[5,6] and more recently starting from Co(II) in ammonium chloride aqueous solutions.[7,8] Details of electrodeposition, including the influence of the coordination sphere on the mechanism of the cobalt nucleation, were included in these publications.[7,8] Reports on black cobalt electrodeposition, however, have yet to define the mechanisms involved. McDonald[9] reported that the black cobalt coating is formed by cobalt(II) oxide when it is electrodeposited from a Watts-type electrolytic bath containing hydrogen peroxide, although he did not describe the electrocrystallization mechanisms for this compound. Smith *et al*.[10] prepared black cobalt using various procedures. One of their better results was achieved in a two-step process where the white metallic cobalt was first deposited on a nickel substrate and then converted to black cobalt through chemical oxidation (in an ammonium persulfate medium). Once again, however, no details of the process were included. Hutchins *et al*.[11] also prepared black cobalt using different techniques, one of which involved electroformation of white cobalt. Once prepared, the white cobalt film was activated in nitric acid aqueous solution to form cobalt nitrate, which, as they attested, facilitated the cobalt oxide or hydroxide formation under a strong alkaline medium (ammonium persulfate). We report here on the deposition mechanism of cobalt onto steel in the presence of nitrates. We found nitrates to be an essential component for direct cobalt electrodeposition, producing black cobalt with excellent photothermal properties.[2]

Experimental

Cobalt film preparation and electrochemical characterization of cobalt film properties.—The kinetics of the cobalt electrodeposition process were studied from a typical electrolytic bath, as described by McDonald[9] and modified as we reported previously.[2] In this study, we used two different electrolytic baths: A, without nitrate to form white cobalt, and B, with the oxidizing agent, NO_3^-, to obtain the black cobalt deposit (see composition in the Table I). An electrochemical study was performed using cyclic voltammetry and potential-step techniques in each of these two baths.

All solutions were prepared with ultrapure, Milli-Q grade water and analytical grade reagents. Experiments were carried out at room temperature in a nitrogen atmosphere. Prior to electrochemical experiments, all solutions were carefully deaerated using clean, nitrogen (99.99% purity) gas.

A conventional three-electrode cell was used for the experiments. As a working electrode (substrate for cobalt deposition), a stainless

* Electrochemical Society Student Member.
** Electrochemical Society Active Member.
z E-mail: igm@xanum.uam.mx

S0013-4651(99)05-090-9 CCC: $7.00 © The Electrochemical Society, Inc.

Table I. Chemical composition of the aqueous electrolytic baths used in this work for white (A) and black (B) cobalt film formation onto stainless steel.

Substance	Concentration (mol L^{-1})	
	A (White cobalt)	B (Black cobalt)
$CoSO_4$	0.98	0.98
$CoCl_2$	0.28	0.28
H_3BO_3	0.20	0.20
KNO_3	0.00	0.10

steel (SS) square (type 304) with a 1.0 cm^2 surface area was embedded in an epoxy resin in such a way that only one phase was exposed to the solution. A graphite rod was utilized as the counter electrode and a saturated calomel electrode (SCE) as the reference electrode. Prior to each experiment, the working electrode surface was polished to a mirror finish with several grades of alumina powder and treated in pure water in an ultrasonic bath for 3 min. During the experiments, the working electrode potential was controlled by means of an EG&G model 263-A potentiostat-galvanostat coupled to a personal computer using *Echem* software. This device provided experimental control and data acquisition.

Cobalt film characterization by SEM-WDX, AFM, and XRD.—Surface characterization of the metallic coating was obtained by X-ray diffraction (XRD) using a Siemens D500 difractometer with Cu Kα radiation. We used scanning electron microscopy (SEM) to observe the overall properties of the cobalt films prepared in an electrolyte solution with and without nitrate. This study was carried out using a SEM Carl Zeis DSM 940A microscope coupled to a WDX detector. In this work, WDX measurements were taken in the wavelength (λ) range of 1.14 Å < λ < 94.36 Å. An atomic force microscope (AFM), Nanoscope III, Digital Instruments, USA) operating in air (*ex situ* experiments) was used to visualize the detailed structure of the cobalt film. To determine and define the cobalt film for quantitative morphological characteristics (surface roughness, estimation of the average grain size, etc.), the multimode software package accompanying the Nanoscope III was used. Measurements were carried out by "contact" in air using standard geometry silicon nitride probes (Digital Instruments). All images are shown in the so called "height mode," where higher areas appear brighter.

Results and Discussion

Cobalt Deposit Characterization

Scanning electron microscopy.—Figure 1 shows two SEM images of the stainless steel substrate surfaces covered with white (Fig. 1a) and black (Fig. 1b) cobalt. Cobalt was electrodeposited onto the stainless steel substrate by means of cathodic potential steps from the two aqueous solutions, A and B (see Table I). The electrodeposition potentials were based on a previous study.[2] In the absence of nitrates (Fig 1a), the deposit is compact while with the addition of nitrates, the deposit consists of dispersed particles (Fig. 1b). Both samples still possess traces of the polishing lines (long-range scratches due to the polishing procedure), indicating that the cobalt layer is not thicker than approximately 0.3 μm. The white cobalt film appears smooth, more like a 2D film, and compact, which indicates association among the deposited particles. In some regions, defects in the form of small pits were observed.

Characterization of surface morphology of cobalt films by AFM.—Although AFM imaging provides more surface structural details than SEM, the technique served mainly to verify our conclusions from SEM imaging. Figure 2a shows the morphology of the stainless steel substrate consisting mainly of large grains, with clearly visible grain edges. This texture is completely lost after formation of the cobalt film. The AFM analysis also showed that the black cobalt film (Fig. 2b) consisted of small nanoclusters, unlike the white cobalt film (Fig. 2c) which is a dispersed 2D film with some occasional clusters. Interestingly, cobalt clusters found on both surfaces were almost equal in size (approximately 150 to 250 nm in diam). From a macroscopic point of view, it is also interesting to estimate the surface roughness for the clean and cobalt covered substrate. Surface roughness, expressed as rms, the root-mean-square function[12-14] is defined as the standard deviation for the height of all imaged features. In this analysis all image points are taken into account. Black and white cobalt possesses significantly different rms values of 69 *vs*. 40 nm, respectively. This

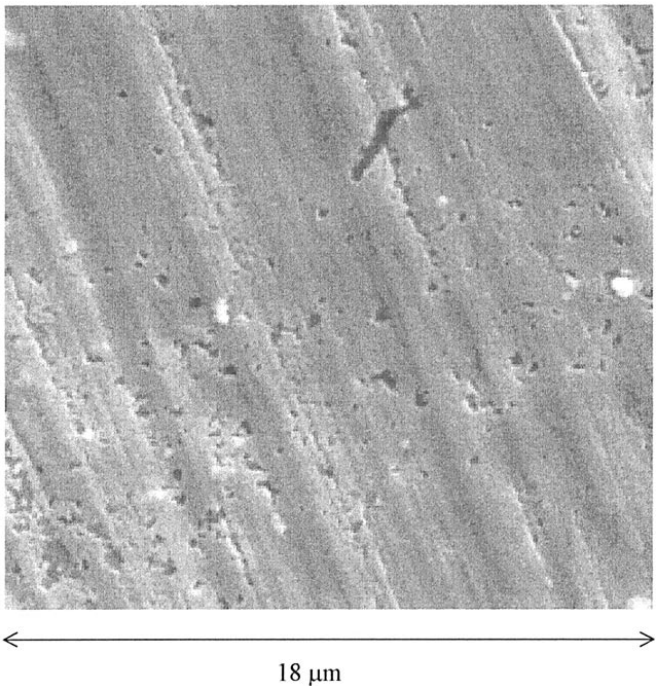

Figure 1. SEM images (times 5000) of the stainless steel (SS) surfaces covered with white (a, top) and black (b, bottom) cobalt. Cobalt was electrodeposited onto the SS substrate by means of a cathodic step (−1.1 V *vs.* SCE for 15 s) from an aqueous solution containing 1.17 M Co(II), 0.98 M H_2SO_4, 0.56 M KCl, and 0.2 M H_3BO_3 in the absence (a) and presence (b) of 0.1 M KNO_3.

S0013-4651(99)05-090-9 CCC: $7.00 © The Electrochemical Society, Inc.

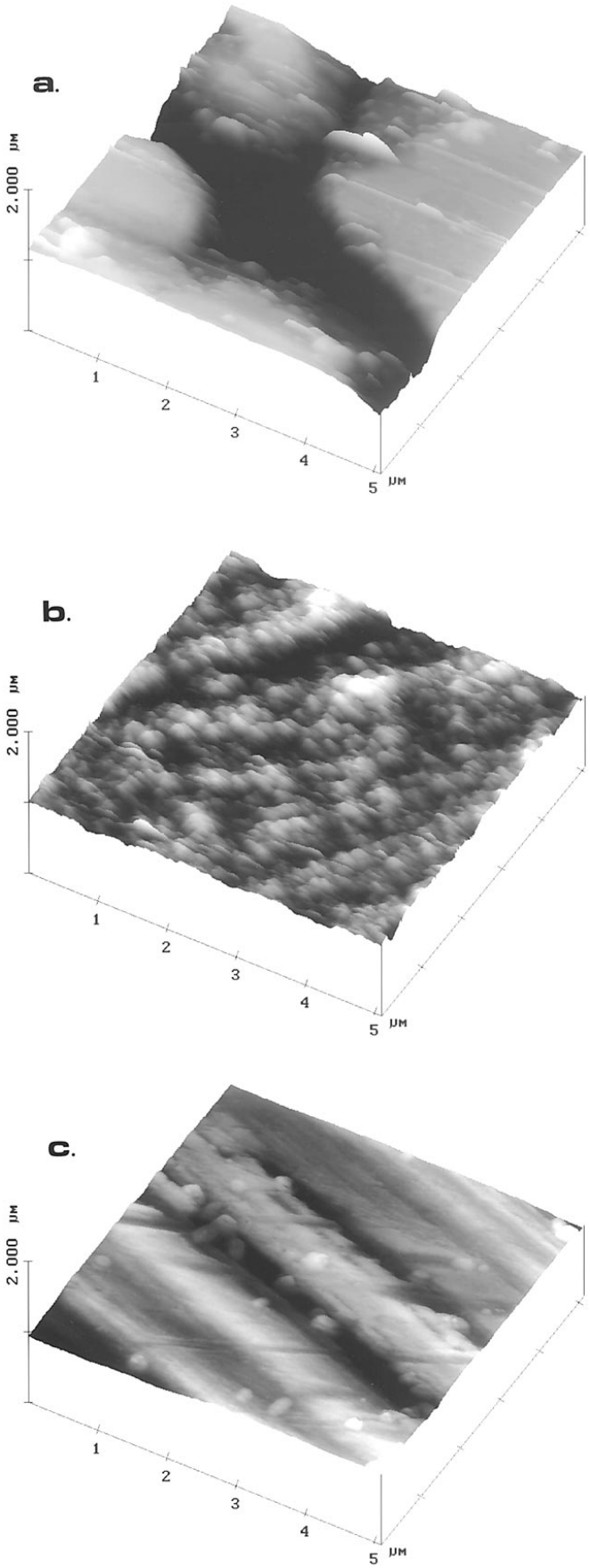

Figure. 2. AFM images of the SS substrate surfaces (a) bare surface, (b) covered with black cobalt deposit, and (c) with white cobalt deposit. The metallic cobalt deposits were obtained under the same conditions of Fig. 1.

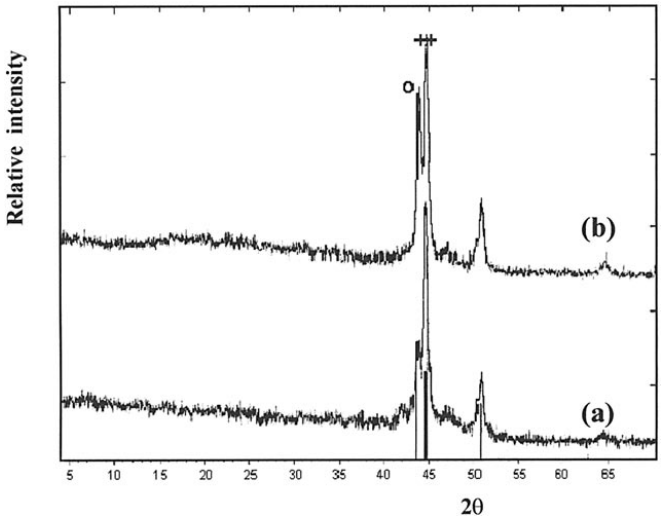

Figure 3. XRD patterns of SS substrates surfaces covered with (a) white cobalt and (b) black cobalt. The standard patterns are shown from (111) and (002) γ-austenite (fine line) and (002) metallic cobalt (bulk line). The lines used for estimates of the fraction of steel surface coated with cobalt are also marked: (ooo) γ-austenite and (+++) cobalt.

is quantitative confirmation of previous morphological observations that the black cobalt, cluster-like film, is rougher than the deposited white cobalt. The white cobalt deposit is more uniform, with a higher fraction of the substrate surface covered, than that of black cobalt.

X-ray diffraction.—We analyzed the chemical composition of white and black cobalt films using (XRD) techniques. Figure 3 shows the two diffraction patterns obtained for white (Fig. 3a) and black (Fig. 3b) cobalt film coatings.

These XRD patterns revealed that in both cases the films were composed of metallic cobalt. When the deposit was formed in the absence of nitrates (solution A), the film was colored, white-gray, and in the presence of small quantities of nitrates (solution B), it was black. Comparison between diffraction peak intensities due to cobalt (002) and that corresponding to the substrate (steel) allowed estimation of the fraction of the steel surface coated with cobalt. We found that white cobalt occupied approximately twice the substrate surface area as black cobalt. Two important features are thus confirmed by these results. The formation of black cobalt films was indeed obtained directly after Co(II) ion reduction from an aqueous solution containing small amounts of NO_3^-, and this black film was composed of dispersed metallic cobalt. This last feature is an essential characteristic for good photothermal efficiency. To our knowledge this is the first report of direct black metallic cobalt formation, since in previous articles[11,12] a black cobalt film was reported as forming indirectly and its composition was related to the formation of cobalt oxide rather than metallic cobalt.

WDX analysis.—In order to confirm the chemical composition of the cobalt deposits, WDX measurements were performed. Figure 4 shows a WDX spectrum for black cobalt deposit (an identical WDX spectrum was obtained for white cobalt deposit). This spectrum shows lines for cobalt and other elements corresponding to the 304 stainless steel substrate (Fe, Cr, Ni). The small lines ($\lambda = 23.5$ Å) assigned to oxygen (see insets in Fig. 4) does not allow the establishment of the presence of oxide compounds in the deposit film. Therefore, white and black cobalt deposits were solely formed by metallic cobalt.

Electrochemical Study

Cyclic voltammetry.—Figure 5 shows two typical voltammograms recorded during cobalt electrodeposition onto stainless steel from solutions (A) and (B). In the cathodic zone ($E < -0.8$ V) of these voltammograms, the Co(II) reduction process produced different voltammetric characteristics depending on the chemical compo-

S0013-4651(99)05-090-9 CCC: $7.00 © The Electrochemical Society, Inc.

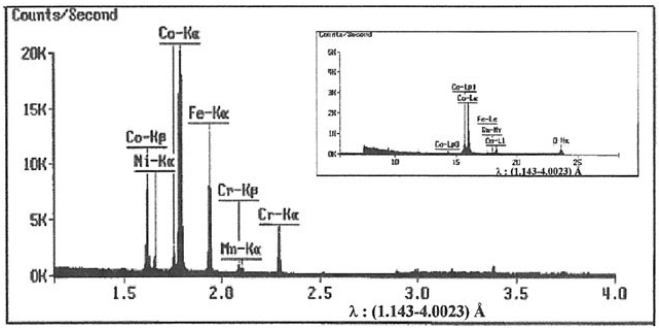

Figure 4. Typical WDX spectrum for the black cobalt deposit onto 304 SS substrate in the wavelength (λ) region of 1.14 Å < λ < 4.0 Å. Insets show a different λ range, 5 Å < λ < 30 Å.

sition of the electrolytic bath. While the cobalt reduction process from solution (A) occurred without the formation of a voltammetric peak (Fig. 5a), for black cobalt deposition, this process developed a well-resolved, voltammetric reduction peak (II′) (Fig. 5b).

In order to show that peak II′ is actually due to cobalt deposition, in Fig. 6 is shown a set of voltammograms obtained at different cathodic switching potentials ($E_{-\lambda}$). Note that in all cases an associated stripping wave is always present. Moreover, the cathodic peak current (II′) varies linearly with the $v^{1/2}$ (v = scan rate potential), indicating the presence of a mass-transfer process.

Note in Fig. 5 that, during the reverse potential scan (from −1.5 to 0.6V), a crossover on the cathodic branches was observed in both cases. This feature indicates that cobalt deposition proceeds via a nucleation and growth phenomena whether nitrates are present in the electrolytic bath or not.[6,8] When the applied potential reached more positive values, in both cases the presence of anodic peaks (I and I′) was observed. These peaks are related to oxidized cobalt deposited during the direct cathodic potential scan. To analyze the cathodic efficiency of the cobalt deposition, we performed a voltammetric study with different cathodic switching potentials ($E_{-\lambda}$), see Fig. 6.

Charges due to the cathodic (Q_c) and anodic (Q_a) processes can be obtained from integration of the cathodic and anodic branches of the *I-E* curves, respectively. Figure 7 shows plots of the Q_a/Q_c ratio as a function of $E_{-\lambda}$ for cobalt deposition from solutions A and B. In the case of the nitrate free solution (white cobalt formation), the Q_a/Q_c ratio reached a value of 1 as $E_{-\lambda}$ became more negative. This indicates that cobalt deposited during the cathodic sweep potential is totally oxidized during the anodic scan. In contrast, the Q_a/Q_c ratio for black cobalt formation (solution B) reached a maximum value of 0.5 for the more negative value of $E_{-\lambda}$ considered. The difference between the anodic and cathodic charges ($Q_c = 2Q_a$) observed in this case could be explained in terms of some process coupled to the cathodic reaction. In other words, this evidence supports the simultaneous presence of another cathodic process (that can consume electrons or recently deposited cobalt) besides cobalt reduction. The main characteristic of this second process is that its charge-transfer product cannot undergo oxidation during the anodic scan. Since the only difference between the deposition baths is the presence of nitrate, it is likely that an interaction between newly deposited cobalt and nitrate ions in solution is occurring in bath B. This interaction could include a direct redox reaction and/or nitrate reduction on the surface of the cobalt nuclei. The former reaction would consume the cobalt deposit, and the latter would provide electrons to the external circuit. Together or separately, these reactions explain the low cobalt recovery efficiency recorded for black cobalt formation. The cobalt deposition processes were studied quantitatively by employing the double potential-step technique.

Potential-step technique.—We analyzed the stability of deposited metallic cobalt performing a double potential pulse study in both deposition baths. Several reduction potentials (E_r) were considered, with the inverse anodic pulse constant (E_a = 0.6 V). The reduction potential range (E_c < −0.9 V) was chosen based on the cathodic zone of the corresponding voltammogram. Metallic cobalt is completely oxidized in both cases (see Fig. 5) at potential values more positive than 0.2 V. Figure 8 shows two typical potentiostatic current transients (*I-t* curves) recorded during white cobalt (Fig. 8a) and black cobalt (Fig. 8b) formation. During the first 20 s a cathodic potential (E_c = −1.1 V) was imposed to the substrate surface followed at t > 20 s by an anodic potential (E_a = 0.6 V). The current-time evolution associated with each applied potential differed depending on the chemical composition of the electrolytic bath. This feature indicates that different mechanisms could be associated with cobalt deposition from the two media.

Integrating each *I-t* curve derived from this potential program, we calculated the charges associated with reduction (Q_c) and oxidation (Q_a) processes during the potential steps. Figure 9 plots the Q_a/Q_c ratio as a function of the cathodic potential step. Once again, cobalt deposition from the electrolytic bath without nitrates resulted in a ratio approximately equal to 1 at all applied cathodic potentials (see Fig. 9a). For black cobalt deposition (solution B), however, the ratio was lower (Fig. 9b). This agrees completely with the voltammetric study and supports the hypothesis proposed above for a cobalt-nitrate interaction. In fact, these observations are similar to those described

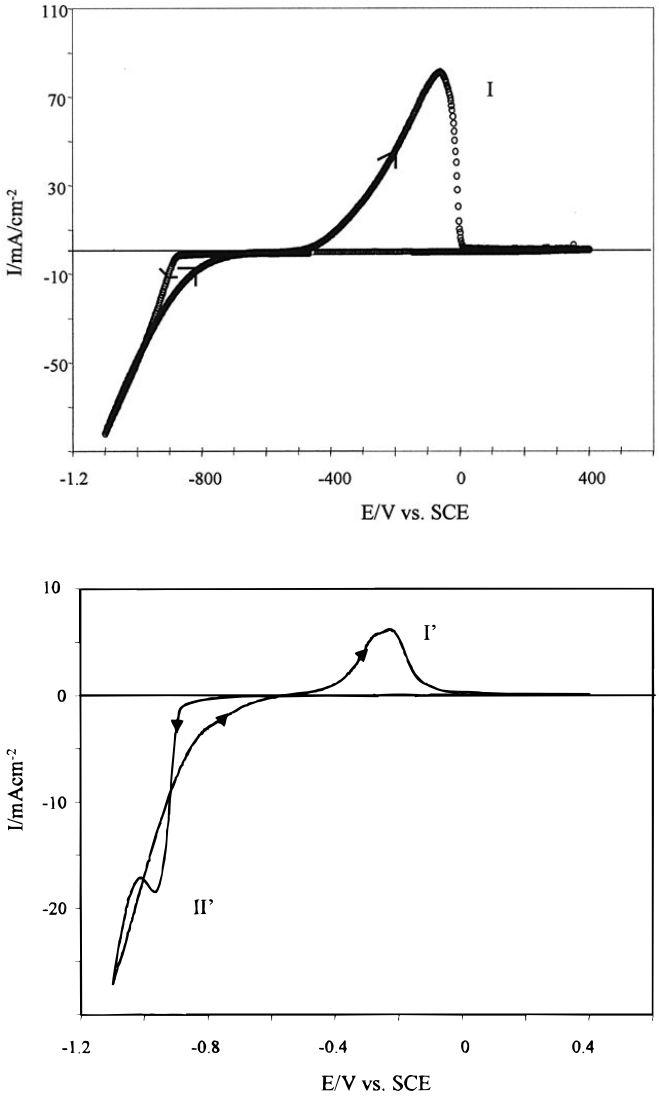

Figure 5. Typical cyclic voltammograms obtained during cobalt deposition onto the SS electrode from an aqueous solution containing 1.17 M Co(II), 0.98 M H_2SO_4, 0.56 M KCl, and 0.2 M H_3BO_3, (a, top) in the absence (white cobalt) and (b, bottom) in the presence (black cobalt) of 0.1 M KNO_3. The scan rate was 20 mV s^{-1}. Peaks related with cobalt deposition (II′) and oxidation (I, I′) are also shown.

S0013-4651(99)05-090-9 CCC: $7.00 © The Electrochemical Society, Inc.

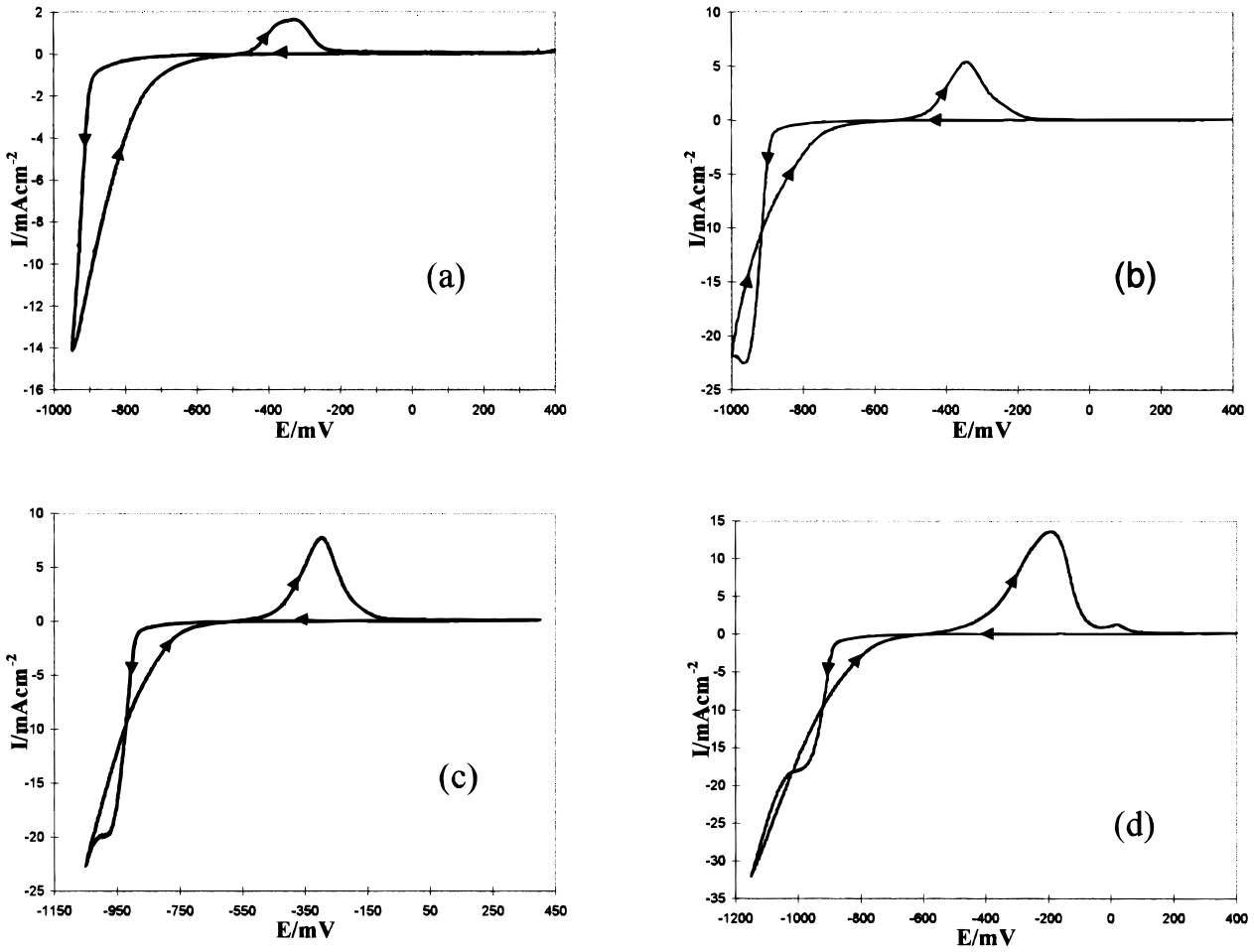

Figure 6. Typical voltammograms obtained on a SS substrate in a 1.17 M Co(II) aqueous solution containing 0.98 M H_2SO_4, 0.56 M KCl, 0.2 M H_3BO_3, and 0.1 M KNO_3 for different cathodic switching potentials ($E_{-\lambda}$). (a) −0.95, (b) −1.0, (c) −1.05, and (d) −1.15 V. The scan rate potential was in all cases 20 mV s^{-1}.

by Serruya and Scharifker,[15] who reported an electrochemical interaction between nitrates in solution and recently deposited thallium on a vitreous carbon electrode.

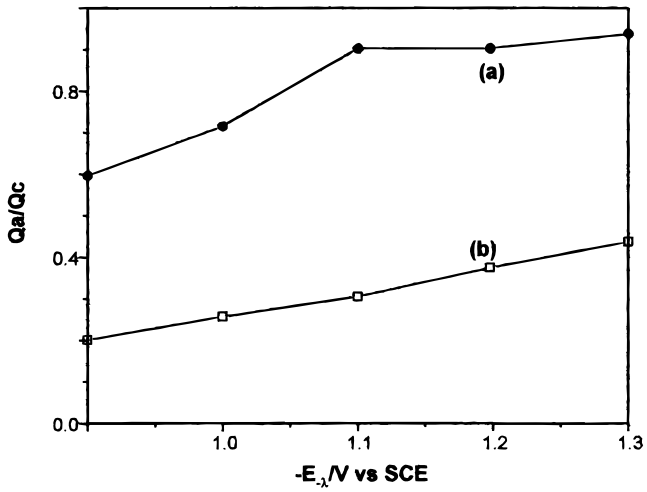

Figure 7. Charge ratio associated to the cathodic (Q_c) and anodic (Q_a) voltammetric branches (see Fig, 6), as a function of the cathodic switching potential ($-E_{-\lambda}$). The charges were evaluated from voltammograms obtained from 1.17 M Co(II) aqueous solution containing 0.98 M H_2SO_4, 0.56 M KCl, 0.2 M H_3BO_3, (a) in the absence (white cobalt) and (b) in the presence (black cobalt) of 0.1 M KNO_3.

Cobalt electrodeposition mechanism.—To confirm the nitrate reaction on recently formed cobalt, we imposed a potential program to the working electrode, as shown in Fig. 10. A reduction potential pulse (E_r) was initially applied during time, t_r. The cell circuit was subsequently opened in order to relax the diffusion layer during a waiting time (t_w), given by ($t_w = t - t_r$), followed by an anodic

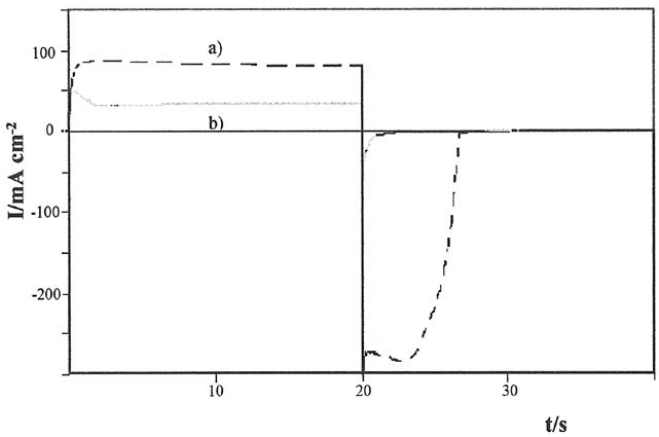

Figure 8. Typical double-potential step current transient obtained in the SS electrode from 1.17 M Co(II) aqueous solution containing 0.98 M H_2SO_4, 0.56 M KCl, and 0.2 M H_3BO_3, (a) in the absence (white cobalt) and (b) in the presence (black cobalt) of 0.1 M KNO_3. The imposed potentials are: E_c = −1.1 V *vs.* SCE, (t < 20 s) and E_a = 0.6 V *vs.* SCE (t > 20 s).

S0013-4651(99)05-090-9 CCC: $7.00 © The Electrochemical Society, Inc.

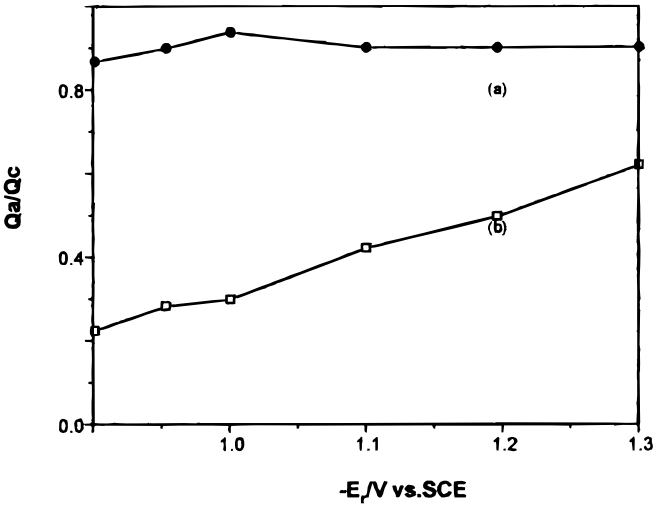

Figure 9. Charge ratio associated to the cathodic (Q_c) and anodic (Q_a) *I-t* curves, as a function of the cathodic potential ($-E_r$) imposed to the SS electrode during the direct pulse. The charges were evaluated from the double-potential step current transients (see Fig. 6). The potential imposed in the reverse pulse was always the same (E_a = 0.6 V). (a) White cobalt and (b) black cobalt deposition.

potential pulse (E_a) imposed during time, t_a ($t_a = t_f - t$) to oxidize the remaining metallic cobalt on the surface.

This experiment was carried out for different waiting times (t_w) in both deposition baths. For each experiment, we calculated the charge (Q_c) associated with the direct E_r potential pulse and the charge (Q_a) due to the applied oxidation potential (E_a). Figure 11 shows the waiting time dependence of the Q_a/Q_c ratio. In the free nitrate bath, the Q_a/Q_c ratio was found to be approximately equal to 1 (Fig. 11a), regardless of the waiting time (t_w) value. When nitrate was added to the cobalt deposition bath, the Q_a/Q_c ratio was highly dependent on t_w, and as t_w increased, the Q_a/Q_c ratio decreased considerably (Fig. 11b). These results support the presence of a redox reaction between the recently formed cobalt deposit and nitrates in solution.

We propose that the following reactions take place during the deposition of cobalt onto a stainless steel substrate from both electrolytic baths.

White cobalt formation, bath A, proceeds via the faradaic Reaction 1

$$Co^{2+}_{(aq)} + 2e^-(\text{steel}) = \text{Co/steel} \quad [1]$$

Black cobalt deposit, bath B, occurs according to the following faradaic (2 and 4) and chemical Reaction 3

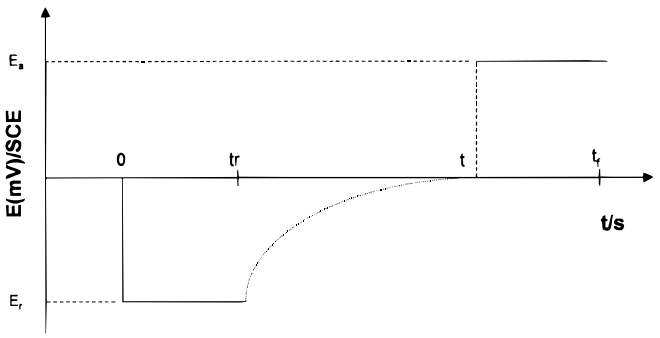

Figure 10. Illustration of the potential step program imposed to the SS electrode, in order to study the stability of the freshly deposited cobalt in the electrolytic baths here considered. The reduction potential (E_r) was initially applied during time t_r. The cell circuit was opened during a waiting time, $t_w = (t - t_r)$ followed by an anodic potential pulse (E_a) applied during the time t_f-t.

$$Co^{2+}_{(aq)} + 2e^-(\text{steel}) = \text{Co/steel} \quad [2]$$

$$2H^+_{(aq)} + NO^-_{3(aq)} + \text{Co/steel} = Co^{2+}_{(aq)} + NO^-_{2(aq)} + H_2O_{(l)} \quad [3]$$

Considering Reaction 3, we propose simultaneous nitrate reduction during the cathodic process according to the following reaction

$$2H^+_{(aq)} + NO^-_{3(aq)} + 2e^-(\text{Co}) = NO^-_{2(aq)} + H_2O_{(l)} \quad [4]$$

Reactions 3 and 4 were proposed based on the solution pH and thermodynamic diagrams of predominant species of the nitrate-nitrite system.[16]

Electrochemical nucleation of cobalt on stainless steel.—The potentiostatic technique has been demonstrated as a powerful tool for elucidating formation mechanisms of new phases (electrocrystallization).[17-22] As nitrates play a major role in the formation of cobalt coatings with photothermal properties (black cobalt), analysis of the electrocrystallization mechanism of Co(II) on steel must be well defined in order to apply such methods reliably. Figures 12 show a current family of potentiostatic transients obtained during white (Fig. 12a) and black (Fig. 12b) cobalt coating formation, respectively.

During white cobalt deposition, the recorded current transient (Fig. 12a) developed a current, which increased over time until reaching a stationary value (plateau). These transients clearly possess the major characteristic of a three-dimensional (3D) nucleation process limited by lattice incorporation of adatoms.[17] For black cobalt formation (Fig. 12b), the experimental transients differed from those observed for white cobalt, with the presence of one (lower overpotential) and two (higher overpotentials) current maxima clearly observed. Formation of the black cobalt deposit thus involves a different mechanism than white cobalt formation, and these mechanisms are now described.

White cobalt formation mechanism.—Experimental potentiostatic current transients obtained during white cobalt formation (Fig. 12a) were fit to Eq. 5, proposed by Armstrong *et al.*[17] This equation describes a 3D nucleation limited by incorporation of adatoms. It is important to note that this model or a variation of it has been successfully applied to the quantitative and qualitative description of the deposition process of a number of experimental systems[23-35]

$$I_{3Di-Li}(t) = P_1[1 - \exp(-P_2t^2)] \quad [5]$$

where

$$P_1 = zFK'_g \quad [6]$$

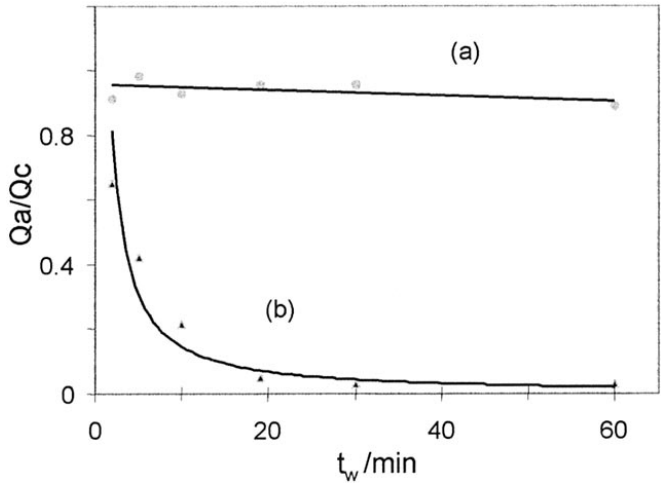

Figure 11. Charge ratio associated to the cathodic (Q_c) and anodic (Q_a) *I-t* curves, as a function of the waiting time (t_w). The charges were evaluated from the current transients obtained with the potential step program shown in Fig. 8. The program was applied to the SS electrode in 1.17 M Co(II) aqueous solution containing 0.98 M H_2SO_4, 0.56 M KCl, and 0.2 M H_3BO_3, (a) in the absence (white cobalt) and (b) in the presence (black cobalt) of 0.1 M KNO_3.

S0013-4651(99)05-090-9 CCC: $7.00 © The Electrochemical Society, Inc.

$$P_2 = \frac{\pi M^2 N_0 K_g^2}{\rho^2} \quad [7]$$

zF is the metallic ion molar charge, K_g' and K_g are the growth rate constants, perpendicular and lateral to the surface, respectively. M is the molar mass, ρ the atomic density of the deposit, and N_0 is the numeric density of active sites on the substrate surface.

Figure 13 shows a comparison between an experimental current transient obtained during white cobalt formation and a theoretical transient generated with Eq. 5. The values of the parameters P_1 and P_2, which give the best fit between these curves, were calculated by nonlinear adjustment of Eq. 5 to the experimental data, as described elsewhere.[21] Theoretical and experimental data observed here are in satisfactorily accord, so that this case is also applicable to the other transients of Fig. 12a.

The kinetic parameter values (P_1 and P_2) obtained using this adjustment are shown in Table II. Note that, while the P_1 values slightly depend on the applied potential, the P_2 values vary exponentially with it. From Eq. 6 and P_1 values, the perpendicular growth rate constants (K_g'), for each applied potential, are easily obtained and in this case, they are in the range of (1.71-6.3) × 10^{-7} mol cm^{-2} s^{-1}, which is within the order of magnitude for other analogous systems.[21,23] However, the independent evaluation of N_0 and K_g is not possible, see Eq. 7. Considering the P_1 and P_2 dependence with the applied potential, and assuming that K_g in this system should have similar values as K_g' (4×10^{-7} mol cm^{-2} s^{-1}), it is then possible to evaluate N_0 from P_2 values. The N_0 values estimated by this way vary exponentially with the applied potential (see Fig. 14). This exponential relationship between N_0 and the applied potential, has been reported by others researches,[18] using independent estimation of N_0.

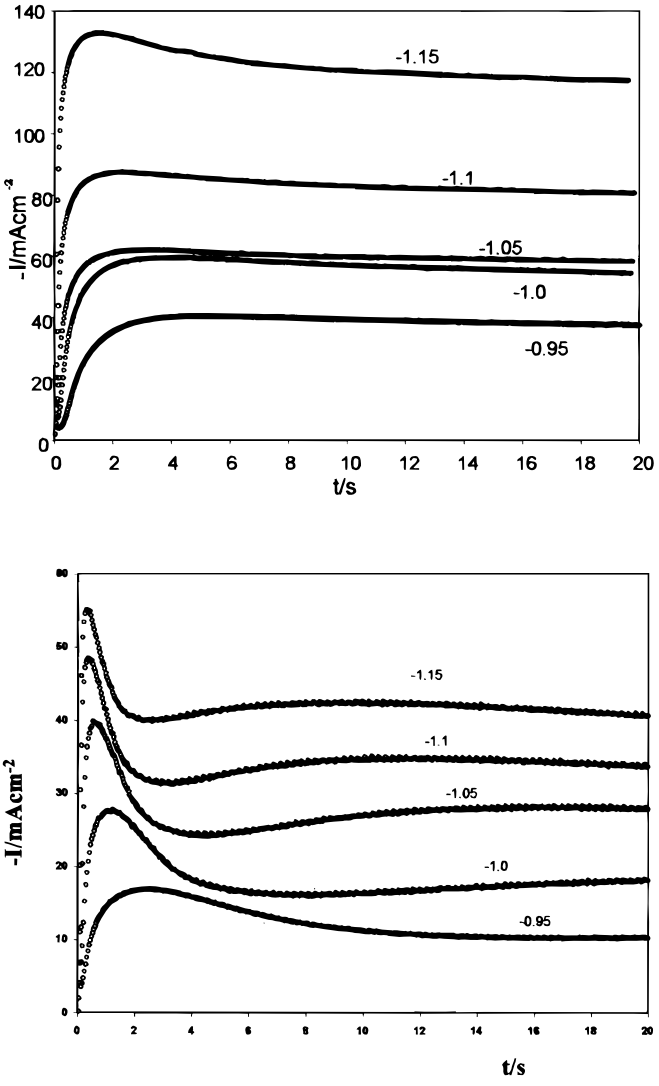

Figure 12. Typical potentiostatic current transients obtained during the white (a, top) and black (b, bottom) cobalt eletrodeposition on stainless steel, from an electrolytic bath containing 1.17 M Co(II), 0.98 M H_2SO_4, 0.56 M KCl, and 0.2 M H_3BO_3 with different KNO_3 concentration (a) 0 M and (b) 0.1 M. The imposed potentials (in volts *vs.* SCE) are shown in the figures.

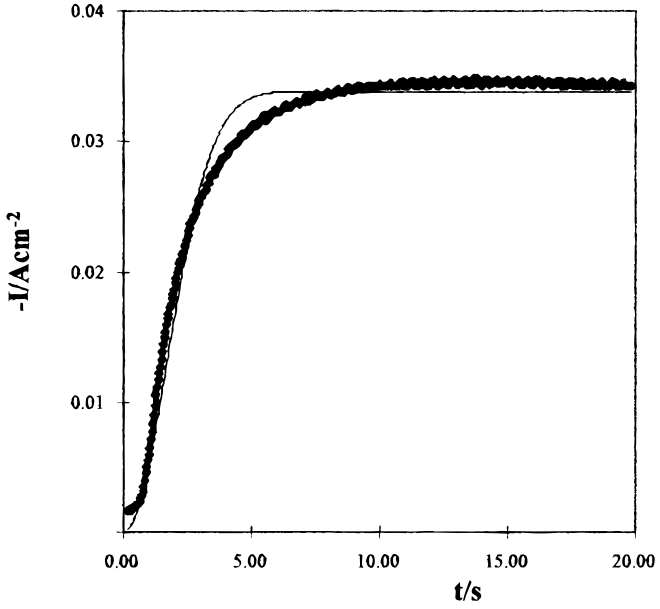

Figure 13. Comparison of an experimental current transient (•••) obtained during the white cobalt formation onto SS substrate surface at an imposed potential of −0.95 V *vs.* SCE (see Fig. 12a) and a theoretical current transient (—) obtained from a nonlinear fitting of Eq. 5 to the experimental data. The fitting parameters were $P_1 = 0.033$ A cm^{-2} and $P_2 = 1.12$ s^{-2}.

Black cobalt formation mechanism.—It is easy to recognize two different cobalt deposition behaviors for the black cobalt electrocrystallization process based on the shape of the experimental potentiostatic current transients (Fig. 12b). Those obtained at less cathodic reduction potentials possess a single current maximum, yet for the most cathodic applied potentials ($E < -1.05$ V *vs.* SCE), recorded transients clearly show two current maxima. Unlike white cobalt formation, black cobalt deposition involves current transients with complex shapes, rarely considered in the literature. The complex shape of these experimental transients could be related to the simultaneous presence of cobalt and nitrate reduction and cobalt-nitrate interactions (Eq. 2-4). Apparently, cobalt-nitrate interactions are more important at higher cathodic potential values, as predicted from the shape of the current transient obtained under these conditions. Although quantitative analysis of the experimental current transients in

Table II. Kinetic parameters of white cobalt deposition on stainless steel obtained from nonlinear fit of experimental *i-t* curves (Fig. 12a) to Eq. 5.

	3Di-li	
$-E$ (V)	P_1 (A cm^{-2})	P_2 (s^{-2})
0.95	0.033	1.12
1.00	0.056	3.2
1.05	0.059	10.13
1.10	0.083	28.36
1.15	0.122	72.04

S0013-4651(99)05-090-9 CCC: $7.00 © The Electrochemical Society, Inc.

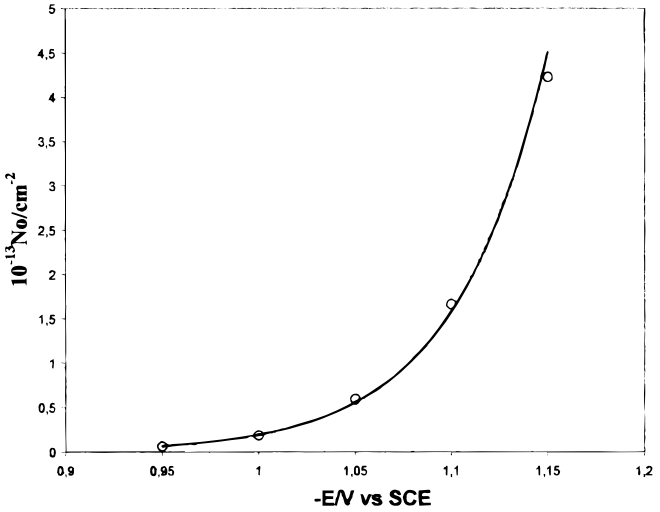

Figure 14. Potential dependence of the numeric density of active sites (N_0) for white cobalt nucleation onto stainless steel (o) evaluated from Eq. 7, the P_2 parameter values reported in Table II and assuming a constant value of $K_g = 4 \times 10^{-7}$ mol cm^{-2} s^{-1}. The continous line represents the exponential adjustment of the experimental data.

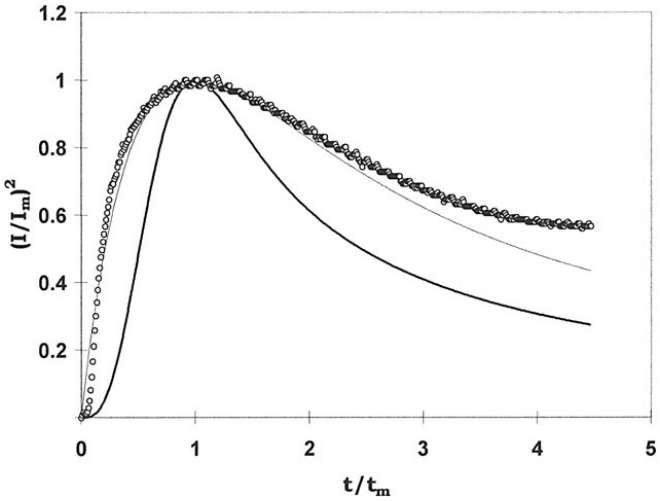

Figure 15. Comparison of the theoretical nondimensional plots $(I/I_m)2$ *vs.* t/t_m for instantaneous (upper curve) and progressive (lower curve) nucleation (see Ref. 18) with experimental data (ooo). The experimental transient was obtained during black cobalt deposition at an imposed potential of −0.95 V *vs.* SCE (see Fig. 12b).

this case is quite complex, we present a new proposal to describe quantitatively the potentiostatic current transient due to a nucleation process, accompanied with a concurrent reaction, at low cathodic potential values. Analysis of current transients obtained at higher cathodic potential will be discussed elsewhere.[36]

Black cobalt formation at low cathodic potentials.—Taking in to account the existence of a current maximum in the experimental current transients obtained during black cobalt formation at less cathodic potentials and the general form of these transients, we decided to perform an analysis in the framework of the theoretical formalism developed by Scharifker *et al.*[18,19] This model describes the 3D nucleation process limited by a mass-transfer reaction. According to this approach,[18] it is possible to distinguish between two kinds of nucleation mechanisms. Instantaneous and progressive nucleation are differentiated by comparing the experimental transient, previously normalized through the coordinates of the current maximum (I_m and t_m), with the theoretical plots due to instantaneous and progressive nucleation[7,8,18] as shown in Fig. 15. From this figure it is clear that instantaneous nucleation describes a large part of the experimental current transient, however, a complete adjustment does not exist, particularly for $t > t_m$.

It is, therefore, necessary to propose a more complete model describing the whole current transient and taking into account the processes described by Eq. 2-4. However, as only the reactions in Eq. 2 and 4 account for electron consumption from the external circuit, we propose to deconvolute the total current in terms of Eq. 8. This proposed mechanism involve the simultaneous presence of a multiple, three-dimensional cobalt nucleation growth, limited by diffusion of cobalt ions ($I_{3D\text{-}dc}$, Eq. 9[18-20]) with nitrate reduction onto cobalt nuclei surfaces (I_{NR}, Eq. 14[22]). This is a particular case of a most general model proposed for deconvolution of complex current transient due to simultaneous faradaic processes[8,19-22]

$$I = I_{3D\text{–}dc} + I_{NR} \quad [8]$$

where

$$I_{3d\text{–}dc}(t) = (P_3 t^{-1/2})\theta \quad [9]$$

with

$$\theta = \left\{1 - \exp\left[-P_4\left(t - \frac{1 - \exp(-P_5 t)}{P_5}\right)\right]\right\} \quad [10]$$

$$P_3 = \frac{zFD^{1/2}c}{\pi^{1/2}} \quad [11]$$

$$P_4 = N_0 \pi k' D \quad [12]$$

$$P_5 = A \quad [13]$$

and

$$I_{NR}(t) = P_6\theta \quad [14]$$

with

$$P_6 = z_N F K_N \quad [15]$$

In these equations, θ is the surface coverage of the formed nuclei,[19] K_N corresponds to the nitrate to nitrite electrochemical reduction constant, (Eq. 4), z_N is the number of electrons involved during this reduction, and F is the Faraday constant. This electrochemical reduction is carried out on the recently deposited cobalt nuclei. D is the cobalt diffusion coefficient, and K is the constant determined by the experimental conditions.[18]

The deposition process for black cobalt (at low cathodic potential) was analyzed using Eq. 8. Kinetic parameters (P_3, P_4, P_5, and P_6) were obtained as a result of the best fit (nonlinear regression) of Eq. 8 to experimental data (see Table III). Figure 16 compares an experimental current transient obtained during black cobalt formation to a theoretical transient generated from Eq. 8. Individual contributions to the total current of the two processes involved are also presented. The theoretical curves describe the experimental data adequately. From the above analysis of the experimental current transient for cobalt deposition, it is important to note that the presence of nitrate in the electrolytic bath changes the limited step for cobalt electrocrystallization, from charge transfer (in the absence of KNO_3) to mass transfer (in presence of 0.1 M KNO_3). Therefore it should be expected that there is a higher limited current in the diffusion-limited cathodic current (black cobalt deposition) than in the case of white cobalt deposition, for the same applied potential; since Co(II) concentration and electrode surface area are the same in both plating systems. However, a simple comparison of the experimental current transients in Fig. 13 and Fig. 16 shows a contrary behavior. This fact indicates the nitrate in the electrolytic bath could play another role in the electrolytic process of cobalt. In order to elucidate this matter, the influence of nitrate concentration on the potentiostatic cobalt deposition was studied.

S0013-4651(99)05-090-9 CCC: $7.00 © The Electrochemical Society, Inc.

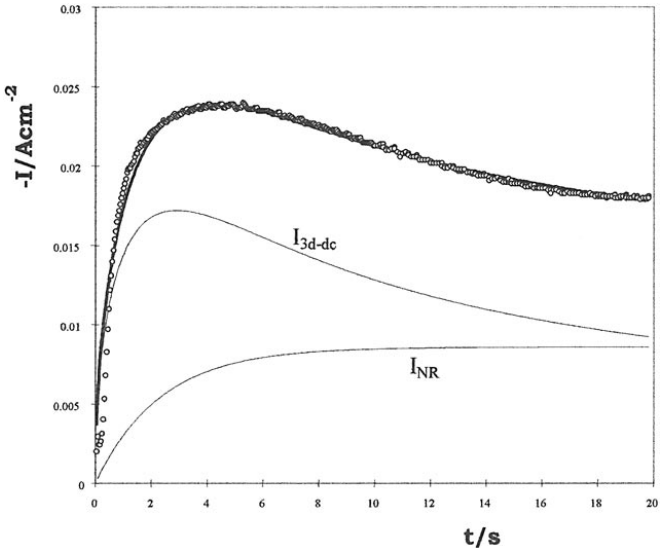

Figure 16. Comparison of an experimental current transient (ooo) obtained during the black cobalt formation onto the SS substrate surface at an imposed potential of −0.95 V *vs.* SCE (see Fig. 12b) and a theoretical current transient (—) obtained from a nonlinear fitting of Eq. 8 to the experimental data. The individual contribution to the total current due to the three-dimensional nucleation process limited by mass-transfer reaction ($I_{3Di\text{-}dc}$) and current associated with nitrate reduction (I_{NR}) over the fresh deposit are also shown. The fitting parameters were P_3 = 37.14 mA cm^{-2} s$^{1/2}$ P_4 = 8.81 s^{-1}, P_5 = 0.51 s^{-1}, and P_6 = 9.49 mA cm^{-2}.

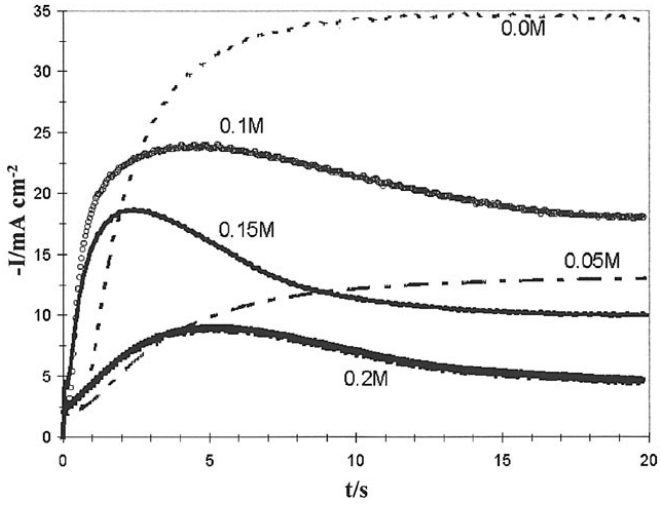

Figure 17. Potentiostatic current transient recorded during cobalt deposition onto SS substrate from an electrolytic bath containing 1.17 M Co(II), 0.98 M H_2SO_4, 0.56 M KCl, and 0.2 M H_3BO_3 with different KNO_3 concentration, indicated in the figure. All transients were recorded at the same applied potential (−0.950 V *vs.* SCE).

Influence of NO_3^- concentration.—Figure 17 shows a set of experimental current transients recorded during the cobalt deposition onto stainless steel substrate electrode from an electrolytic bath containing different KNO_3 concentration, at the same applied potential (−0.95 V). The addition of KNO_3 in the electrodeposition bath drastically changes the shapes of the current transients. For KNO_3 concentrations $C_{KNO3} \leq 0.05$ M, the current transients possess the major features described by the 3D nucleation model limited by lattice incorporation of adatoms (see the section on White cobalt formation), yet for $C_{KNO3} \geq 0.1$ M the current transients show the major features for 3D nucleation limited by mass-transfer reaction, coupled with concurrent nitrate reduction (see the section on Black cobalt formation).

Note that for the nitrate concentration range that induces the transition between lattice incorporation (0.05 M KNO_3) to mass-transfer control (0.1 M KNO_3), the current associated to the mass-transfer controlled electrodeposition process is higher than that associated to charge-transfer control, as it was expected. It is also important to note that for the same limited step for cobalt deposition, the increase of the nitrate concentration provokes a diminution of the associated current to the electrodeposition process.

Therefore the increase of nitrate concentration in the cobalt electrodeposition bath, besides the fact that it provokes a transition of the controlled step, should be modified a common kinetic parameter for both electrocystallization process, for instance, the number density of active sites (*No*). This kinetic parameter was evaluated from the analysis of the current transients.

The current transients obtained in the presence of $C_{KNO3} > 0.1$ M have been analyzed with the same procedure described for the black cobalt deposit formation as noted above. Figure 18 shows a comparison of experimental and theoretical current transients for cobalt electrodeposition in presence of $C_{KNO3} > 0.1$ M. The kinetics parameters obtained for the best fit procedure are shown in Table III. The kinetics parameters for the cobalt electrodeposition in presence of $C_{KNO3} \leq 0.05$ M, were obtained following the procedure described for white cobalt electrodeposition formation as noted above. The resulting fitting parameters (P_1 and P_2) are also shown in Table III.

It is possible to establish that the ratio of P_1 values obtained for 0.0 and 0.05 M KNO_3 can be directly related with K'_g ratio (see Eq. 6). Thus the addition of KNO_3 up to 0.05 M to the electrodeposition bath provokes a diminution of 2.5 times the value of the perpendicular growth rate constant, K'_g. On the other hand, the active sites (associated to P_4 constant) (see Eq. 12) diminish with the increment of KNO_3 concentration, causing a diminution of the cobalt nuclei formed during the electrodeposition; and therefore the cobalt surface area available for NO_3^- reduction is depleting when the nitrate concentration increases (see values of P_6 in Table III).

From the appropriate parameters and the correspondent equation for cobalt electrododeposition mechanism here considered, the number of active sites (*No*) were evaluated. Despite of the use of two different models for this evaluation, the *No* diminishes exponentially with the increase of nitrate concentration over the whole concen-

Table III. Influence of the NO_3^- concentration in the cobalt electrodeposition bath, on the kinetic parameters of cobalt deposition on stainless steel. Kinetic parameters were obtained from nonlinear fit of experimental *i-t* curves in Fig. 17, to Eq. 5, for $[NO_3^-] \leq 0.5$ M and Eq. 8, for $[NO_3^-] > 0.5$ M .

	3Di-li		3D-dc			NR
$[NO_3^-]$ (mol L^{-1})	P_1 (mA cm^{-2})	P_2 (s^{-2})	P_3 (mA cm^{-2} s$^{1/2}$)	P_4 (s^{-1})	P_5 (s^{-1})	P_6 (mA cm^{-2})
0.00	33.00	1.12				
0.05	12.87	0.005				
0.10			37.14	8.81	0.51	9.49
0.15			29.18	4.02	0.90	2.71
0.20			25.85	0.01	0.97	3.67e-8

S0013-4651(99)05-090-9 CCC: $7.00 © The Electrochemical Society, Inc.

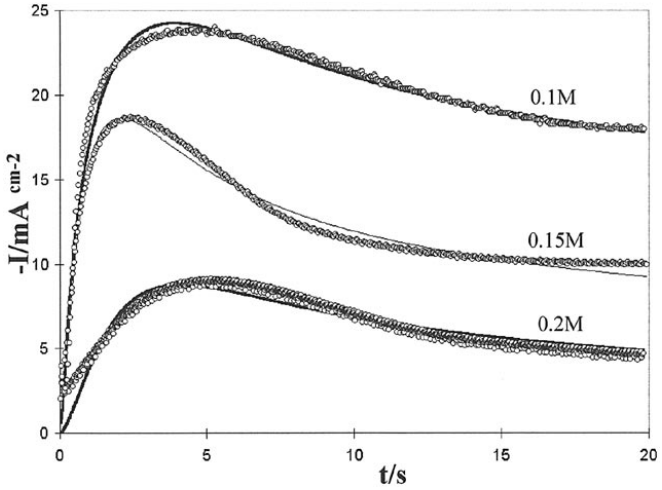

Figure. 18. Comparison of some experimental current transients (oooo) obtained at the same conditions of Fig. 17, with theoretical (—) current transients obtained from a nonlinear fitting of Eq. 8 to experimental data. The kinetic parameters that give the best fit are reported in Table III. The KNO_3 concentrations in the electrolytic bath are indicated in the figure.

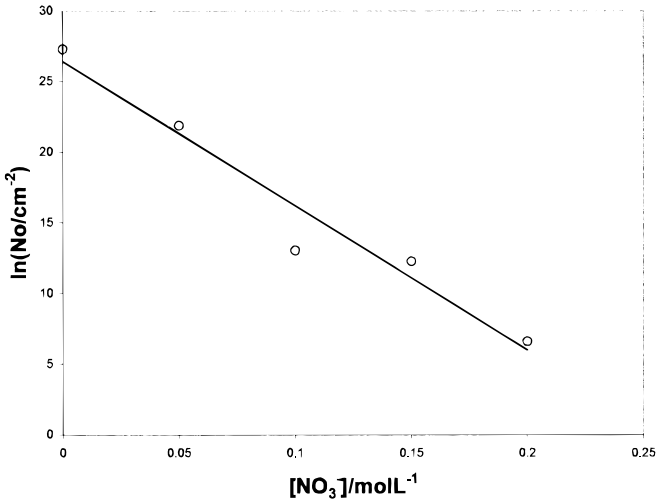

Figure 19. Variation of the number density of active sites (N_0) toward cobalt deposition onto SS, as a function of the KNO_3 concentration in the electrodeposition bath. (o) Experimental results, (—) logarithmic adjustment.

tration range considered (see Fig. 19). Thus, we can conclude that, the nitrate ions can block active sites on the stainless steel substrates toward cobalt nucleation. This phenomenon could be so important that the limiting step for cobalt reduction could be modified and the current associated to cobalt deposition diminished when the nitrate concentration increases.

Conclusions

The addition of a relatively small quantity of nitrate to a cobalt deposition bath (Watts type), results in the electrochemical formation of black cobalt film, instead of white cobalt, which is formed in the absence of nitrate. XRD studies showed that the film deposited in both cases, with and without nitrate in solution, consists of metallic cobalt. Analysis of the deposited cobalt surface by AFM and SEM techniques showed that the black cobalt deposit is more dispersed and less smooth than the white cobalt. Therefore, the appropriate photothermal characteristics of the black cobalt coating are mainly due to its physical surface features (*i.e.*, roughness, coverage capacity, form, and deposited grain size) rather than its chemical nature.

Voltammetric and double-potential step studies showed that different electrocrystallization mechanisms are involved in the white and black cobalt deposition processes. The difference is due to an electrochemical and/or chemical interaction between the nitrate and newly formed metallic cobalt. This interaction provokes a more dispersed and rougher surface for black cobalt as compared to white cobalt deposition.

While white cobalt deposition mechanisms were shown to occur via multiple 3D nucleation, limited by lattice incorporation of cobalt adatoms to the growth centers; the black cobalt was shown to involve the simultaneous process of 3D nuclei formation and growth, limited by mass-transfer reaction, and reduction of nitrates in the medium onto the surfaces of these nuclei. It is shown that besides this cobalt-nitrate interaction, NO_3^- ions in solution can block active sites for cobalt reduction and the effect of this phenomenon strongly depends on the nitrate concentration.

Acknowledgment

This work was carried out with the financial support of CONACYT, projects 400200-5-1776PA and 32158E.

Universidad Autónoma Metropolitana-Iztapalapa and Azcapotzalco assisted in meeting the publication costs of this article.

References

1. F. Trieb, Ph.D. Thesis, DLR Institut fur Technische Termodynamik, Germany (1995).
2. E. Barrera. I. González, and T. Viveros, *Sol. Energy Mater. Sol. Cells*, **51**, 69 (1998).
3. I. M. Croll, *Advances in X-Ray Analysis*, Vol. 4, p.151. Plenum Press, New York (1980).
4. I. M. Croll and B. A. May, in *Electrodeposition Technology, Theory and Practice*, L. T. Romanikiw and D. R. Turner, Editors, PV 87-17 , p. 295, The Electrochemical Society Proceeding Series, Pennington, NJ (1987).
5. L. Brossared, *Mater Chem. Phys.*, **27**, 235 (1991).
6. C. Q. Cui, S. P. Jiang, and A. C. C. Tseung, *J. Electrochem. Soc*., **138**, 1001 (1991)
7. A. B. Soto, E. M. Arce, M. Palomar-Pardavé, and I. González, *Electrochim. Acta*, **41**, 2647 (1996).
8. M. Palomar-Pardavé, I. González, A. B. Soto, and E. M. Arce, *J. Electroanal. Chem.*, **443**, 125 (1998).
9. G. E. McDonald, *Sol. Energy*, **17**, 119 (1975).
10. G. B. Smith, A. Ignatiev, and G. Zajac, *J. Appl. Phys*., **51**, 8 (1980).
11. M. G. Hutchins, P. J. Wright, and P. D. Grebenik, *Sol. Energy Mater.*, **16**, 113 (1987).
12. R. J. Phillips, T. D. Golden, M. G. Shumsky, and J. A. Switzer, *J. Electrochem. Soc.*, **141**, 2391 (1994).
13. W. U. Schmidt, R. C. Alkire, and A. A. Gewirth, *J. Electrochem. Soc.*, **143**, 3122 (1996).
14. D. Aurbach and Y. Cohen, *J. Electrochem. Soc.*, **143**, 3525 (1996).
15. A. Serruya and B. R. Scharifker, in Extended abstracts of the Tenth Congreso de la Sociedad Venezolana de Electroquímica, p. 57 (1997).
16. M. T. Ramírez, Ph.D. Thesis, Universidad Autónoma Metropolitana, México City (1997).
17. R. D. Armstrong, M. Fleischmann, and H. R. Thirsk, *Trans. Faraday Soc.*, **58**, 2200 (1962).
18. B. Scharifker and G. Hills, *Electrochim. Acta*, **28**, 879 (1983).
19. B. R. Scharifker, J. Mostany, M. Palomar-Pardavé, and I. González, *J. Electrochem. Soc*., **146**, 1005 (1999).
20. M. Palomar Pardavé, Ph.D. Thesis, Universidad Autónoma Metropolitana, México City (1998).
21. M. Palomar-Pardavé, M. Miranda-Hernández, I. González, and N. Batina, *Surf. Sci*., **399**, 80 (1998).
22. M. Palomar-Pardavé, B. R. Scharifker, E. M. Arce, and I. González, In preparation.
23. Y. G. Li and A. Lasia, *J. Electrochem. Soc*., **144**, 1979 (1997).
24. U. Schmidt, M. Donten, and J. G. Osteryoung, *J. Electrochem. Soc*., **144**, 2013 (1997).
25. H. C. De Long and R. T. Carlin, *J. Electrochem. Soc*., **144**, 2747 (1995).
26. G. A. Tsirlira, O. A. Petrii, and S. Yu. V. Vassiliev, *J. Electroanal. Chem.*, **414**, 41 (1996).
27. I. B. Burrows, J. A. Harrison, and J. Thomson, *J. Electroanal. Chem*., **58**, 241 (1975).
28. C. Kuhnhardt, *J. Electroanal. Chem.*, **369**, 71 (1994).
29. R. J. Phillips, T. D. Golden, M. G. Shumsky, and J. A. Switzer, *J. Electrochem. Soc.*, **141**, 2391 (1994).
30. F. E. Varela, M. E. Vela, J. R. Vilche, and A. J. Arvia, *Electrochim. Acta*, **38**, 1513 (1993).
31. M. Y. Abyaneh, J. Hendrikx, W. Visicher, and F. Barendrecht, *J. Electrochem. Soc*., **129**, 2654 (1982).
32. M. Y. Abyaneh and M. Fleischmann, *J. Electroanal. Chem*., **119**, 197 (1981).
33. E. N. Codaro and J. R. Vilche, *Electrochim. Acta*, **42**, 549 (1997).
34. M. Y. Abyaneh, *Electrochim. Acta*, **36**, 727 (1991).
35. C. A. Gervasi, F. E. Varela, J. R. Vilche, and P. E. Álvarez, *Electrochim. Acta*, **42**, 537 (1997).
36. E. Barrera, M. Palomar-Pardavé, and I. González, In preparation.